

# Laser-induced fracture in silicon

L. E. MURR, W. A. SZILVA

*Department of Metallurgical and Materials Engineering, New Mexico Institute of Mining and Technology, Socorro, New Mexico, USA*

Utilizing the scanning electron microscope, the laser-impact zone on irradiated P-type silicon wafers has been characterized by a central region of compressive stress which decreases to zero and becomes tensile in character with increasing radius from the impact centre, with symmetrical fracturing occurring around the impact centre at a point of maximum tensile stress. The effect of surface flaws on the fracture of brittle Si wafers and their interaction with the impact zone were observed to be small for scratch widths of 60  $\mu\text{m}$ , and lengths of 1 cm. Direct observations of advancing crack tips were made in the transmission electron microscope, and shown to have associated arrays of partial and total dislocations. The presence of numerous precipitates in the P-type Si wafers possessing long-range strain fields which overlapped along the  $\{111\}$  cleavage planes was observed to have a direct influence on the fracture process. Fracture was observed to occur in wafers containing cleavage-oriented scratches or scratches deviating by  $\sim 5^\circ$  from a cleavage-plane orientation, but little influence was noted for randomly oriented scratches or those which deviated from a cleavage-plane orientation by  $\sim 10^\circ$  or greater.

## 1. Introduction

The interaction of a laser beam with optically transparent and opaque brittle solids is of interest for practical as well as academic reasons, and there have been a number of studies of laser-induced fracture of brittle solids by Q-switched and non-Q-switched laser energy sources [1-4]. Avizonis and Farrington [5] and Agranat *et al.* [6] have shown that internal defects such as inclusions or precipitates can act as localized absorption sites on which the laser energy may be deposited to initiate internal microcracks by the intense local heating which occurs. In addition, energy deposition on an absorbing surface film can give rise to rapid vapourization of the film, resulting in the generation of a pressure pulse which propagates through the solid as an elastic compressive stress wave [7-9]. In the case of a thin wafer, the heated zone which results by laser irradiation produces surface compression which changes to tension on cooling [10].

The present experimental programme was intended to study the effect of flaws on the fracture of brittle silicon (111) single-crystal wafers thermally stressed by a laser beam focused onto the surface for durations up to 5 sec. The experimental samples were large (5 cm diameter)

wafer discs having thicknesses ranging from 200 to 300  $\mu\text{m}$ , so that the surface area to thickness was very large, approximating to some extent a two-dimensional (biaxial) stress system.

There do not appear to have been any similar experiments directed toward an understanding of laser-induced fracture in silicon wafers, or brittle single-crystal materials in general containing surface flaws. The present experimental programme, therefore, has as its purpose the investigation of the influence of systematically oriented surface flaws on the fracture of a brittle wafer, and the investigation of the nature of laser-induced fracture and the associated fracture characteristics in brittle wafers representing an idealized brittle continuum possessing systematic cohesion anisotropies, i.e. cleavage planes.

## 2. Experimental methods

Boron-doped, P-type silicon wafers from [111] pulled crystal boules (Texas Instruments, Inc) having nominal resistivities ranging from 10 to 21  $\Omega\text{cm}$ , 5 cm diameter, and varying in thickness in the final test sample from 200 to 300  $\mu\text{m}$  were employed throughout this investigation. Pure Si wafers of 2.5 cm diameter with a [111] orientation were obtained for structural monitoring

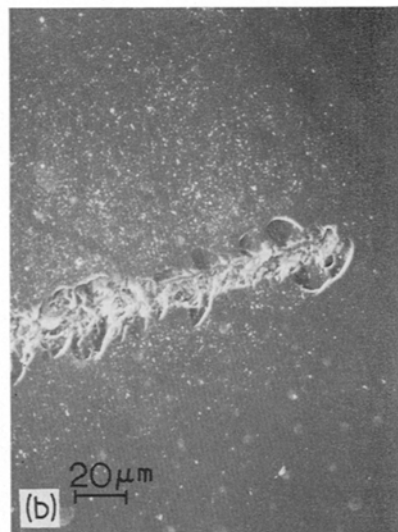
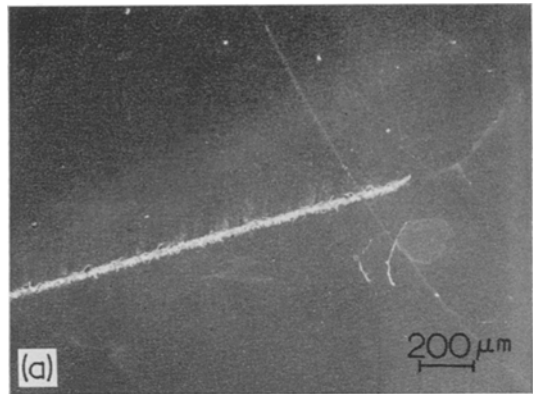
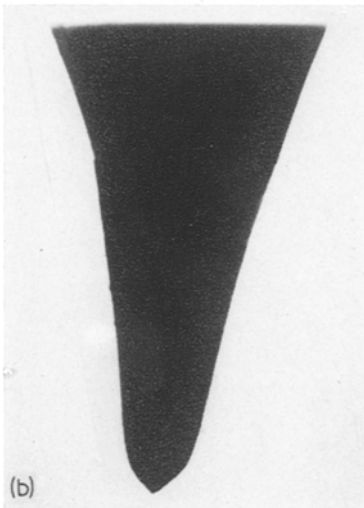
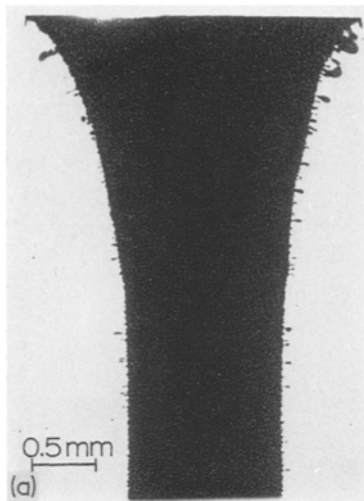


Figure 1 GTE Sylvania 10.6  $\mu\text{m}$  laser burn patterns in plexiglass. (a) Complete burn-through showing approximate beam size. (b) Partial burn through showing beam symmetry and burn profile. (200 W power level.)

purposes. Wafers were either mechanically polished to a fine surface finish on one side and then chemically polished or completely chemically polished to create a final surface.

A technique was developed to systematically isolate wafer sections from any surface region with a specific location accuracy of roughly 0.5

Figure 2 Scanning electron micrographs of typical scratches on the surface of P-type silicon wafers. (a) Scratch flaw, (b) scratch tip, (c) high magnification of flaw structure.

Figure 2

mm, and the chemical etch used in this process was also employed as a short-time surface polish for the test wafers [11].

Surface observations were performed utilizing a Vickers Metallograph and an AMR900 scanning electron microscope. The isolated sections of wafers thinned to electron transparent samples were observed in a Hitachi-Perkin Elmer H.U. 200 F transmission electron microscope operated at 200 kV; utilizing a goniometer tilt stage.

Specimens were irradiated with a GTE Sylvania 971 CO<sub>2</sub> (10.6 μm) laser operated at 200 W, utilizing an external focusing lens to attain a 1 mm spot size on the specimen surface. Irradiation times were varied between 1 and 5 sec; nominal times of 5 sec were used preferentially. In most samples fracture was observed to occur after roughly 5 sec of laser irradiation. The beam size was observed to be roughly 1 mm diameter as illustrated in a typical plexiglass burn pattern in Fig. 1a. Fig. 1b also illustrates a partial burn

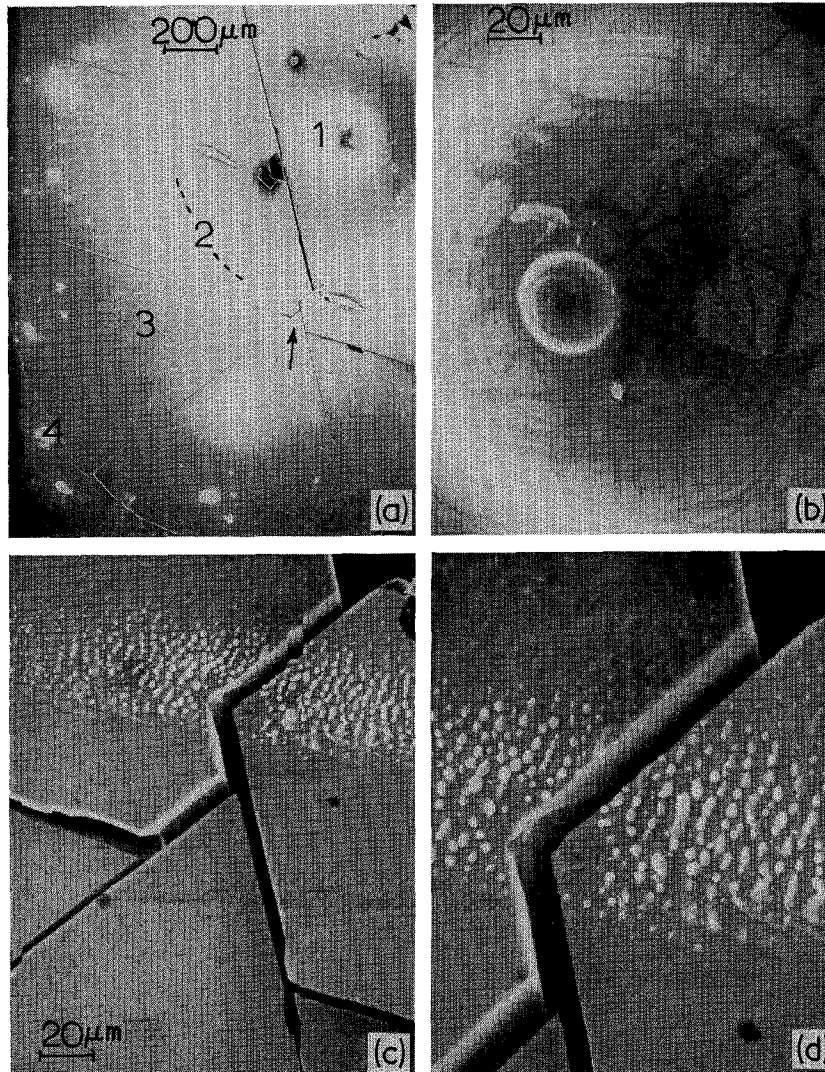


Figure 3 Laser impact zone on a silicon wafer (200 W-5 sec). (a) Low magnification view showing central melt zone (1), vapour redeposition ring (2), deformation zone (3) and terminal crack ring (4). (b) Magnified view of central impact zone (1) in (a). (c) Magnified view of crystallographic cracks (along  $\langle 110 \rangle$ ) at arrow in (a). (d) Magnified view of (c).

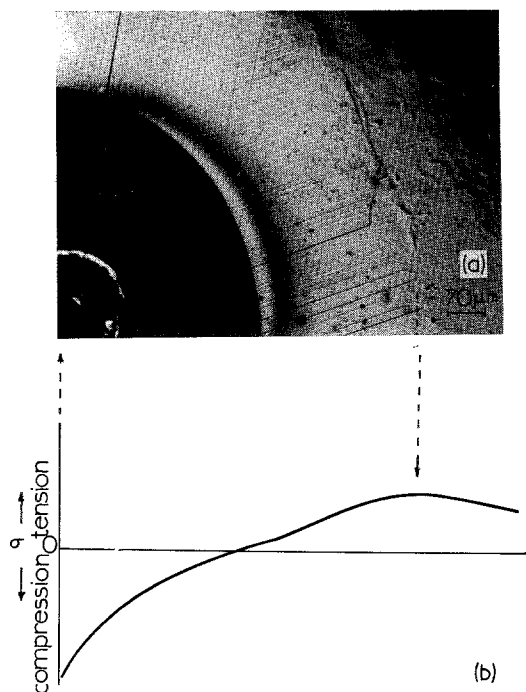


Figure 4 Optical micrograph of laser impact zone and corresponding theoretical stress situation. (a) Micrograph impact of zone similar to Fig. 3a showing slip line field and fracture perimeter. (b) Calculated stress-radius profile corresponding to impact zone in (a).

through in a thicker plexiglass specimen, which illustrates the beam symmetry. An essentially perfect beam symmetry is depicted in Fig. 1. The impact zone and its relationship to experimental surface flaws was established on the test specimens using a low-energy He-Ne laser.

Flaws were placed on the surface of the Si test specimens after establishing a final surface polish, using a metal rule and a diamond stylus which produced an irregular scratch having a width and depth which could be varied according to the exerted pressure. Reasonably consistent scratches were made which measured approximately 50 to 60  $\mu\text{m}$  width and 6 to 10  $\mu\text{m}$  depth, having a structure illustrated typically in Fig. 2. The scratches, measuring approximately 1 cm in length, were placed either along a diameter through the impact point located near the centre of the sample, or along a cord normal to this diameter. The diameter, however, was oriented either along a cleavage plane (in a  $\langle 022 \rangle$  direction) or at some angle to a  $\langle 022 \rangle$  direction.

The scratches were located at various distances from the laser impact zone. In one series of runs the distance was roughly 1 cm, while in another series the distance was reduced to 1 mm.

### 3. Experimental results and discussion

The principal features of the laser impact-zone morphology and fracture-related structural phenomena are illustrated in Fig. 3. The impact zone consists of a melt region (1 in Fig. 3a), with a deposition ring (2 in Fig. 3a), where vapourized Si was redeposited onto the surface in a manner similar to that observed previously for laser damaged Be [12]. Some deformation and fracturing was observed within regions 1 and 2 in Fig. 3a, while the bulk of the deformation appeared to be concentrated in the zone marked 3 in Fig. 3a, and was characterized by a terminal boundary consisting of continuous cracks. Zone 3 (Fig. 3a), while not observable in the SEM, was observed in the metallograph to consist of heavy slip-lines or fault traces terminating on the crack ring (4 in Fig. 3a). These features are illustrated in the optical micrographs in Fig. 4. Only a few cracks were observed to exist beyond the crack zone 4, and those which did appeared to nucleate at the crack zone.

Fig. 4 shows the central impact zone to be characterized by a region of very high compressive stress which decreases radially to zero and then becomes tensile in character. Fracture around the perimeter of the impact zone occurs at the point of maximum tensile stress; slip lines and microcracks propagate predominantly back from this zone (4 in Fig. 3a) in the direction of decreasing tensile stress. The calculated curve in Fig. 4a is based upon a theoretical treatment of Timoshenko's thermal stress model [13, 14]. The prominent conical uprise associated with the impact zone centre could be explained as a response to the intense compressive stress at the centre, and the transition from a melt zone (and some attendant vapourization) to plastic phases which exhibits a viscosity change which reacts to the compressive stress by pushing the molten and plastic material toward the centre, and in a direction of maximum flow (toward the front or impact surface). A smooth cone emerges from the impact (irradiated) surface exhibiting a series of rings. These rings, illustrated typically in Fig. 5, are due to contours of constant dilatation formed along additive lines of principal strains as previously depicted in computed profiles [14]. These contours appear in the scanning electron

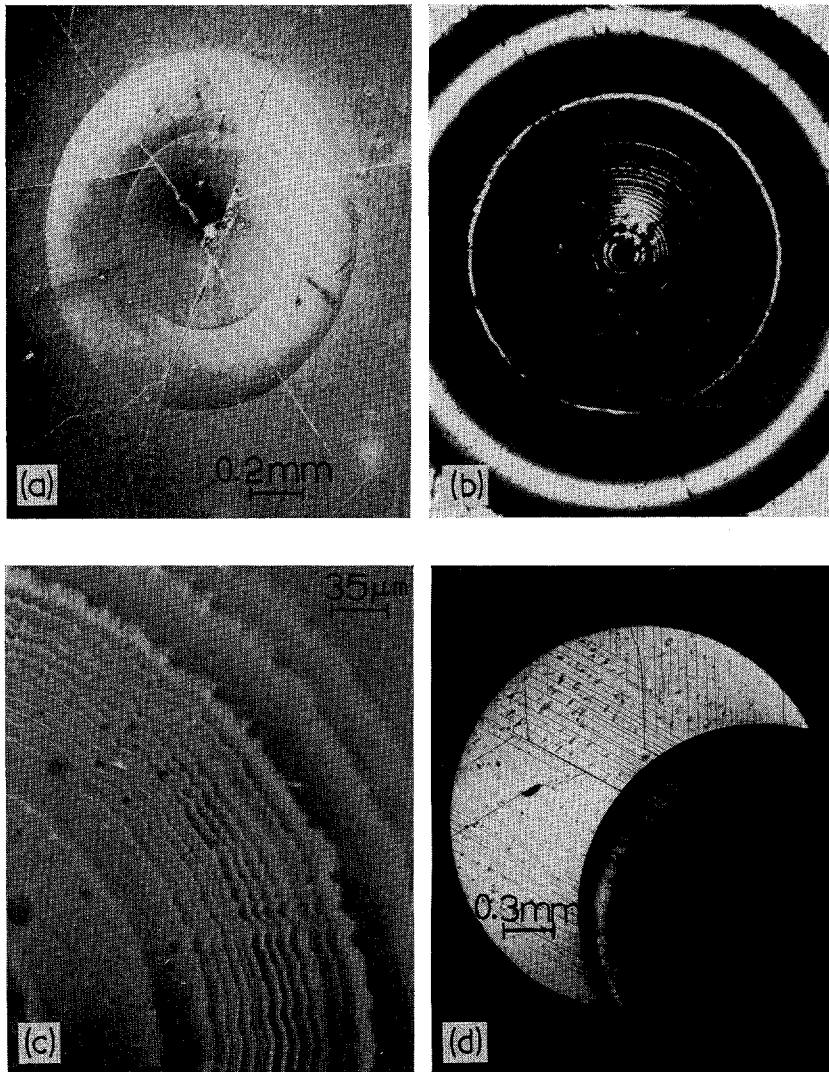


Figure 5 Dilatation contours on the laser impact cone. (a) Scanning electron micrograph of impact cone. (b) Optical micrograph of impact cone. (c) Magnified optical micrograph of dilatation contours. (d) Optical micrograph showing impact cone and cleavage lines associated with cone base.

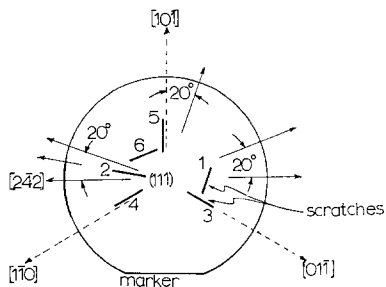


Figure 6 Scratch geometry for laser fracture experiments on Si wafers. Numbers refer to experimental scratch geometries. The cleavage planes are denoted by the  $\langle 011 \rangle$  directions.

microscope as smooth transitions rather than steps, in support of this explanation.

### 3.1. Flaw interaction studies

Figs. 6 to 9 illustrate the results of two series of flaw interaction studies. Figs. 6 and 7 depict scratch geometries and residual damage features of laser-irradiated wafers. It can be observed in Fig. 7 that in wafers which actually fractured, there was no direct interaction with the surface scratches, as evidenced by cracks running through the scratch, but each of the fractured wafers were observed to have scratches which were coincident with a cleavage-plane orientation

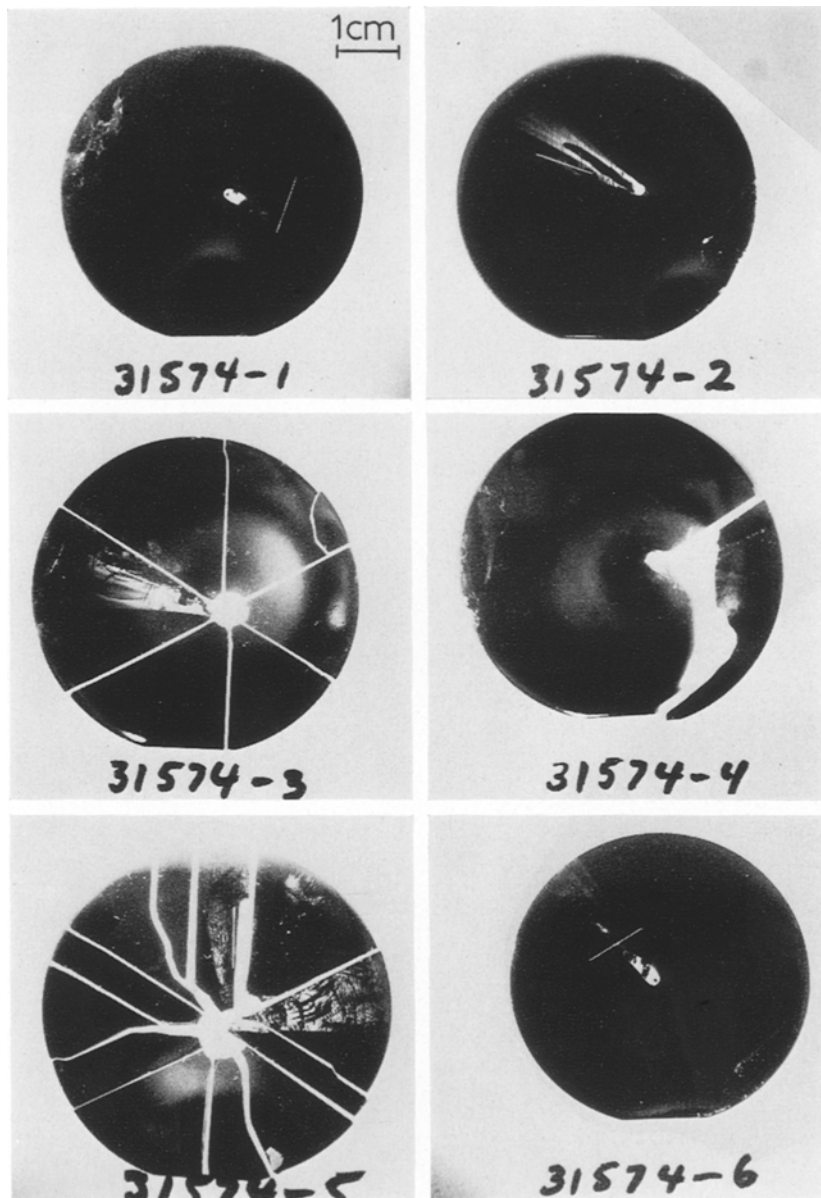


Figure 7 Experimental fracture series: laser-induced fractures in B-doped Si. Reconstructed wafer sections according to the code numbers shown in Fig. 6.

( $\langle 022 \rangle$ ), c.f. Figs. 6 and 7. Detailed examination of the scratch regions in both the scanning and transmission electron microscopes failed to indicate any evidence of dislocation build-up, cracks, or cleavage (slip) traces. There was an apparent lack of direct coupling of the laser-induced fracturing and the scratches, a feature prominently illustrated in sample 31574-5 of Fig.

7. The fracture is in most cases observed to be cleavage fracture, and to be associated in whole or in part with the  $\langle 022 \rangle$  directions ( $\{111\}$  planes).

As shown in Figs. 8 and 9, the scratches were moved closer to the laser impact zone, within the tensile stress region depicted in Fig. 3. In this way, it was assumed that if direct coupling were

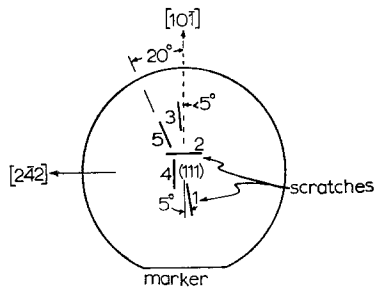


Figure 8 Scratch geometry for laser fracture experiments on P-type Si wafers. Numbers refer to experimental scratch geometries in Fig. 9. Cleavage planes are denoted by the  $\langle 011 \rangle$  directions. The scratch distances from the laser impact zone were roughly 1 mm.

to occur, it would do so within this stressed zone. The results shown in Fig. 9 illustrate that very little interaction between laser-induced cracks and the flaws occurred even for those close-proximity scratches. This feature is illustrated in Figs. 10 and 11, which show the details of scratch-crack interactions, as observed in the

optical metallograph and the scanning electron microscope. Fig. 10a and b show that the scratches cause slight distortion of the cleavage zone (slip zone shown as region 3 in Fig. 3a). However, the scratches do not contribute significantly to fracture in the region in which they intersect the zone, although there is some non-systematic (non-cleavage) cracking associated with the scratches. Fig. 11 shows a magnified view of the scratch in sample 1 of Fig. 9. The by-passing of the scratch by the cleavage crack is clearly illustrated. Again, while there is no strong coupling with the scratch, there is a definite effect on the by-passing cleavage fracture as indicated by the fact that the fracture line runs parallel to the scratch along a major part of its length. In addition, the fractured wafers in Fig. 9 are observed to be either those containing scratches oriented in the cleavage directions or scratches which deviate from a cleavage direction by about  $5^\circ$ . This was also shown previously in Fig. 7. The effect of cleavage-oriented scratches is, therefore, observed to enhance fracture.

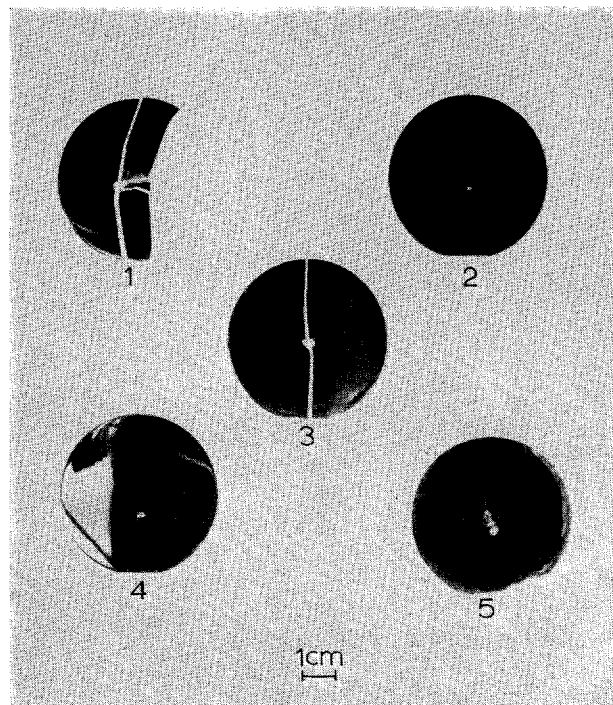


Figure 9 Experimental fracture series corresponding to Fig. 8 Reconstructed wafer sections according to code numbers shown in Fig. 8.

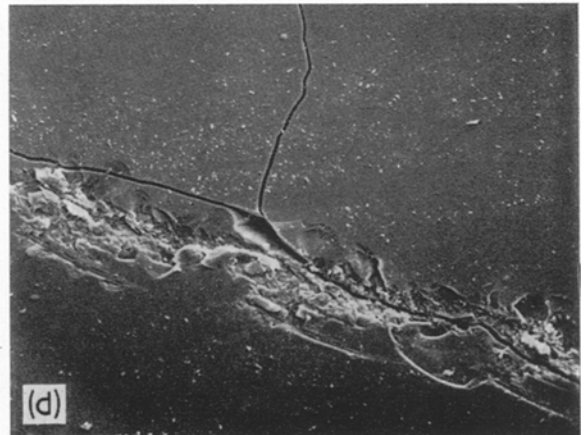
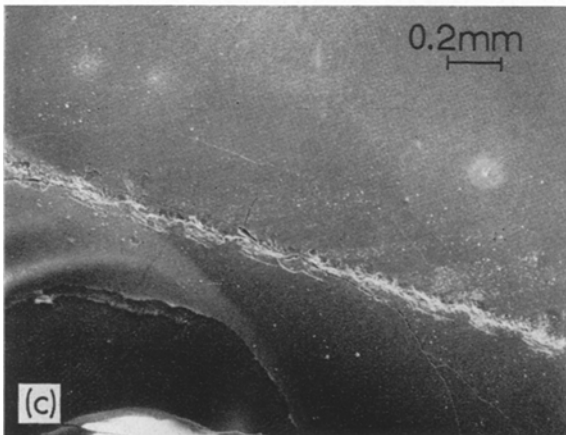
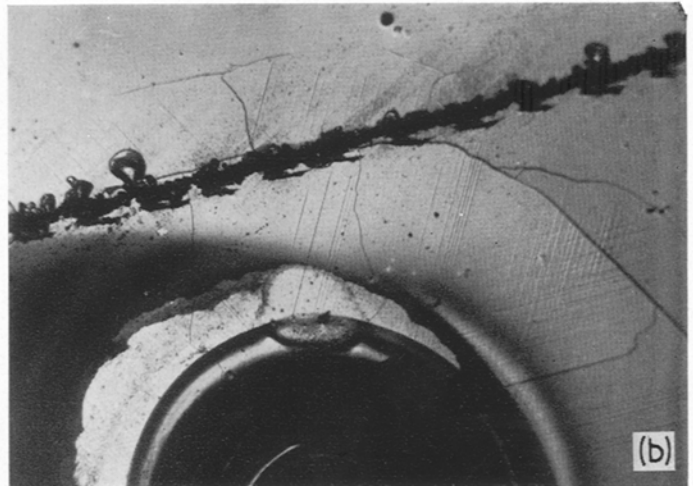
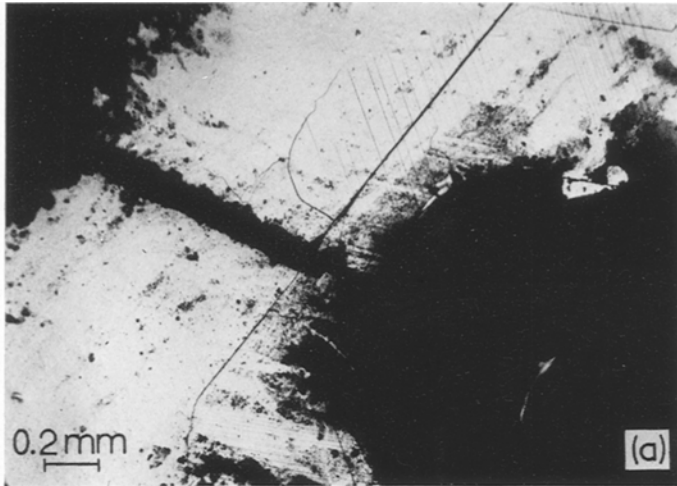


Figure 10 Scratch-crack interactions in laser-irradiated P-type silicon wafers. (a) Diametral scratch extending into impact zone depicted in Fig. 11 (sample 5). (b) Cord-oriented scratch extending into impact zone depicted in Fig. 9 (sample 4). (c) SEM view of scratch-crack interaction zone in (b). (d) Magnified view of (c).

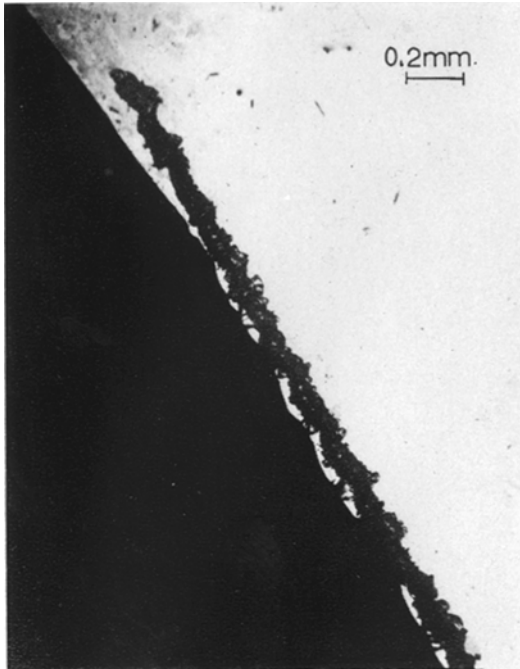
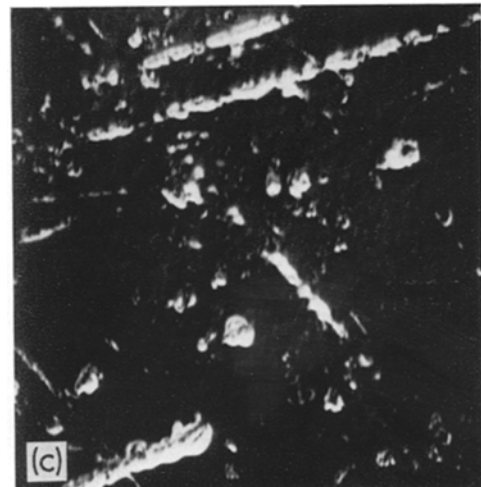
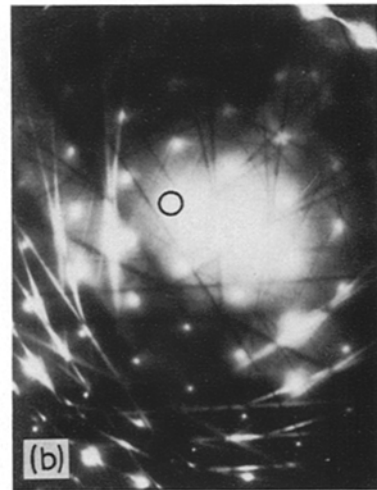
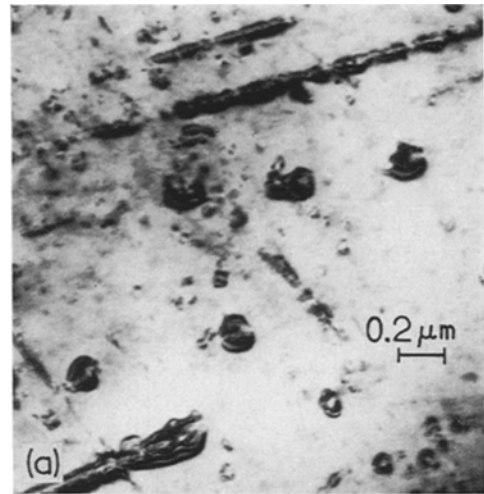


Figure 11 Fracture by-pass of scratch in Fig. 9 sample observed in the optical metallograph.



### 3.2. Internal microstructures and cleavage crack structure

In an attempt to investigate the detailed structure of cleavage cracks and related fracture phenomena in the laser-irradiated P-type silicon wafers, selected-areas from various test specimens were systematically isolated from specific regions over the surface and were examined by transmission-electron microscopy. Fig. 12 illustrates the appearance of the P-type boron-doped silicon wafer specimens following polishing and surface preparation prior to placing a scratch and laser irradiation. The sequence of bright- and dark-field electron micrographs in Fig. 12a and c are indicative of extended arrays of precipitates, presumably borides ( $\text{SiB}_2$ ) oriented along the cleavage planes (in the  $\langle 022 \rangle$  directions). The image reversal in Fig. 12c using a silicon  $\langle 022 \rangle$  matrix reflection, shown circled in (b).

Figure 12 Arrays of precipitates in P-type silicon specimen. (a) Bright-field electron micrograph showing strain-field contrast at linear precipitate arrays. (b) Selected-area electron diffraction pattern of (a). (c) Dark-field electron micrograph of (a) showing strain field contrast reversal and overlapping strain fields using Si  $[022]$  reflection shown circled in (b).

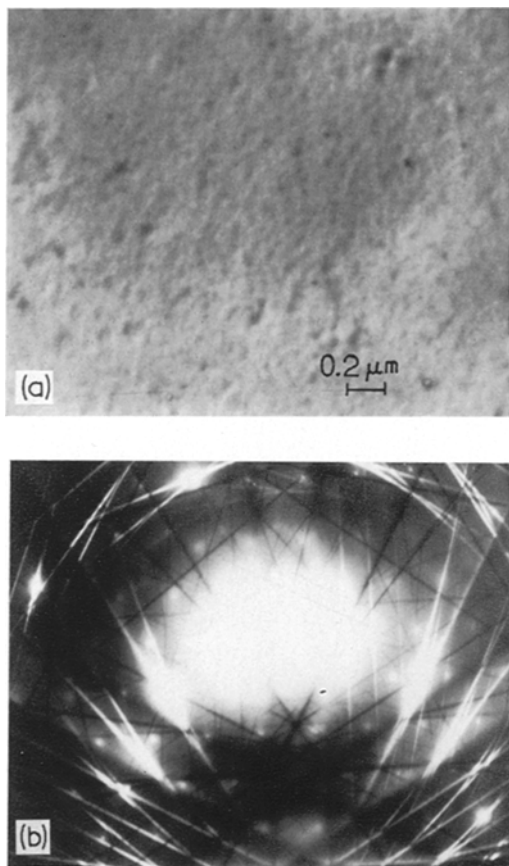
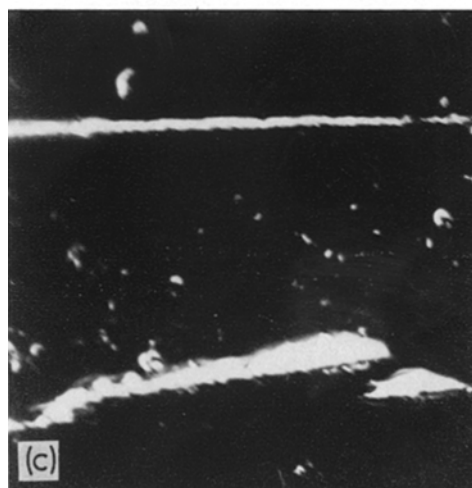
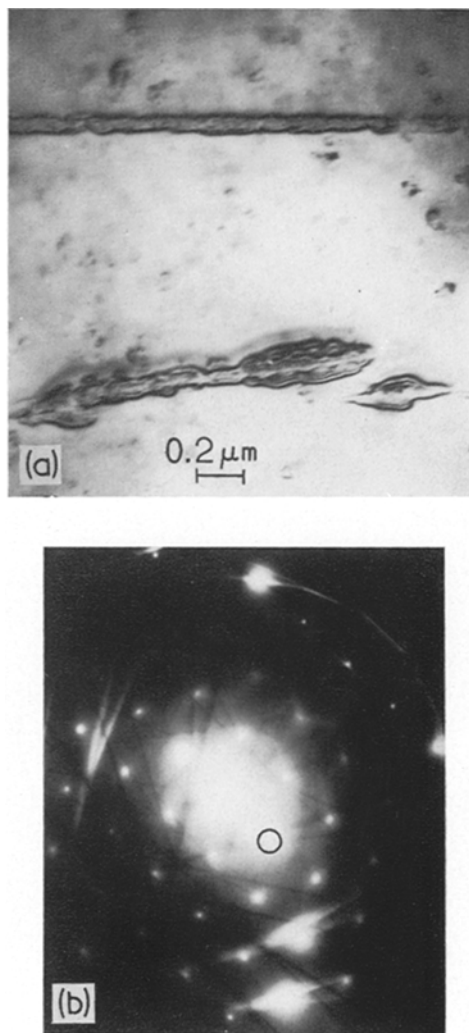


Figure 13 Pure Si wafer section. (a) Bright-field transmission electron micrograph of pure silicon section. (b) Selected-area electron diffraction pattern of (a) showing [111] orientation similar to Fig. 12b.

in Fig. 12b, attests to the occurrence of large, overlapping, strain fields associated with the tiny precipitates. Precipitates in the doped-silicon test wafers were observed as individual particles imaged by their associated strain-field contrast [15]. The density of both individual and continuous linear arrays of precipitates was observed to vary from specimen to specimen, but was usually prominent when compared with the structure (or absence of it) in a pure silicon wafer illustrated for comparison in Fig. 13.

The presence of overlapping precipitate arrays

Figure 14 Closely overlapping precipitate strain fields forming continuous cleavage flaw in doped silicon test specimen. (a) Bright-field transmission electron micrograph. (b) Selected-area electron diffraction pattern of (a). (c) Dark-field image of (a) using  $[0\bar{2}2]$  reflection shown circled in (b).



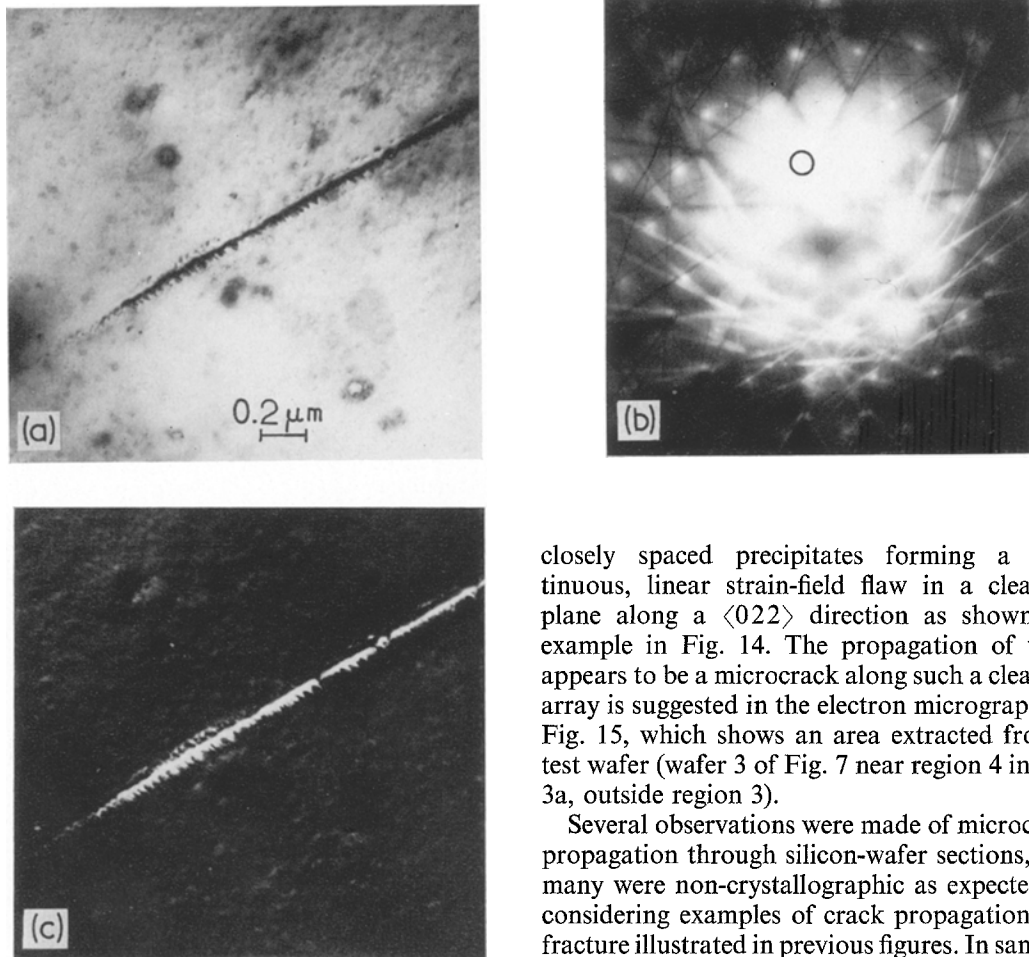


*Figure 15* Apparent microcrack propagation along cleavage plane containing precipitates. (a) Bright-field transmission electron micrograph. (b) Selected-area electron diffraction pattern of (a). (c) Dark-field image of (a) using  $[20\bar{2}]$  reflection circled in (b).

in the P-type silicon specimens, as illustrated in Fig. 12, presented a case of internal microscopic flaws. Since cleavage cracks occur by weakening of bonds along the  $\langle 111 \rangle$  directions in the  $\{111\}$  planes of silicon, the presence of precipitates and associated large strains localized along the cleavage planes would be expected to act as an intrinsic flaw, giving rise to preferential crack-propagation along these linear arrays, or initiated by them. The effects of such intrinsic flaws on crack initiation and fracture would be expected to be enhanced by cleavage-oriented external scratches as observed in Figs. 7 and 9.

Loss of cohesion could be associated with very

closely spaced precipitates forming a continuous, linear strain-field flaw in a cleavage plane along a  $\langle 022 \rangle$  direction as shown for example in Fig. 14. The propagation of what appears to be a microcrack along such a cleavage array is suggested in the electron micrographs in Fig. 15, which shows an area extracted from a test wafer (wafer 3 of Fig. 7 near region 4 in Fig. 3a, outside region 3).

Several observations were made of microcrack propagation through silicon-wafer sections, and many were non-crystallographic as expected on considering examples of crack propagation and fracture illustrated in previous figures. In samples extracted from areas in test wafers near the fracture ring, cracks could be followed into the matrix, and the crack tip examined in detail. Most crack tips were characterized by dislocations (total and partial dislocations) leading the advancing crack. These features are illustrated in the composite transmission electron micrographs shown in Fig. 16. Fig. 16 illustrates the non-crystallographic branching which occurs and the dislocations associated with the advancing crack tip. The crack is observed to be advancing in a heavily precipitated region. It is of interest that dislocations are associated with the advancing crack tip and appear in a form similar to that predicted by classical dislocation theories. It is particularly significant to note that while dislocations have been postulated to accompany crack-tip advance, there have been only a few direct observations of this feature. However, similar results have recently been observed by Bethge [16] at crack tips in MgO.

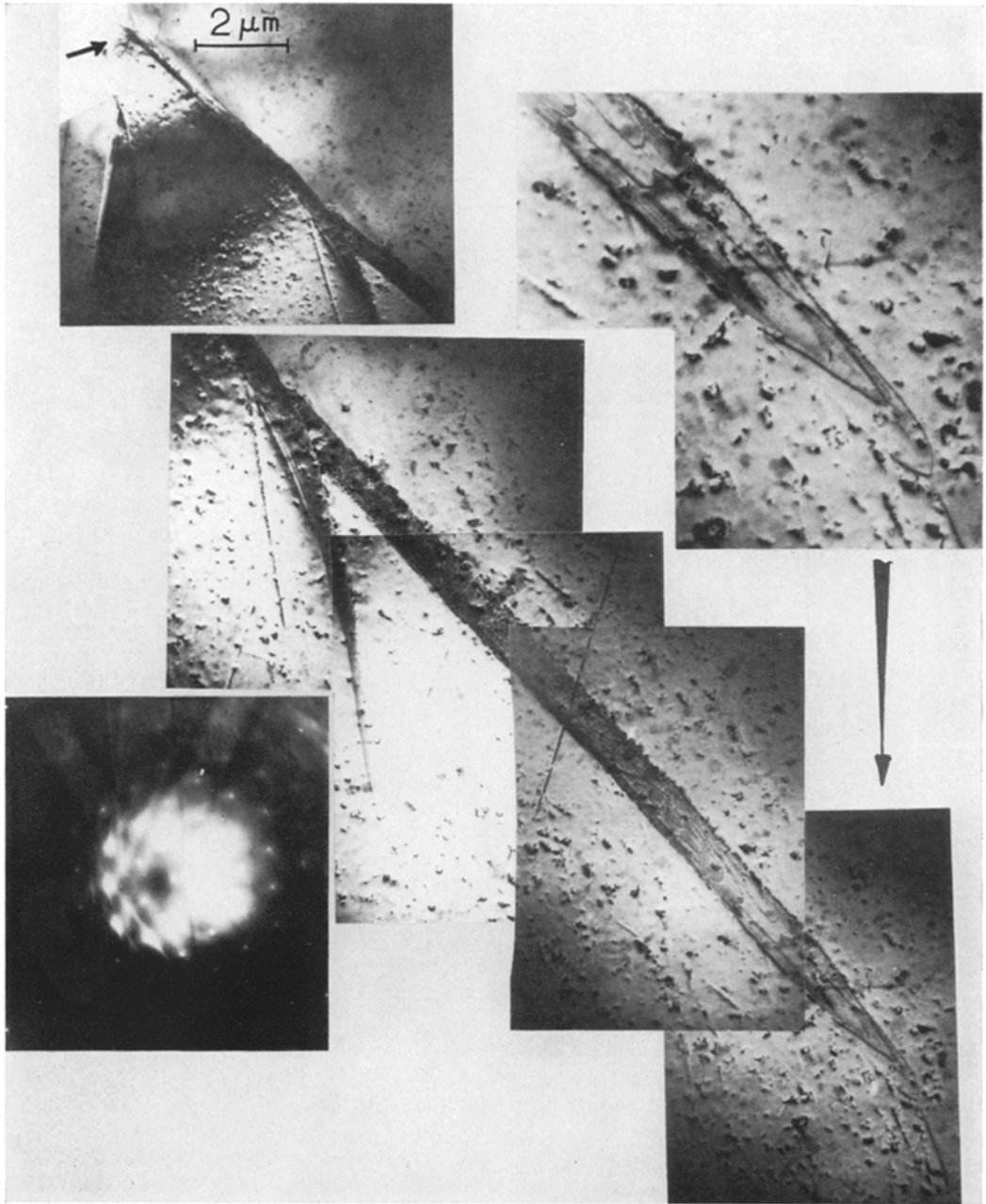


*Figure 16* Transmission electron micrograph composite showing advancing microcrack in P-type boron-doped Si test sample. The crack advances from the edge of the sample (arrow) into the matrix. The crystallographic branch is followed to observe the crack tip, which is composed of dislocations and overlapping stacking faults as illustrated in the magnified insert.

#### 4. Conclusions

The experimental results have yielded some interesting characteristics of laser-induced fracture in P-type silicon single-crystal wafers. The

laser impact-zone has been characterized by regions of compression and tension, with symmetrical fracturing occurring around the impact centre at a point of maximum tensile

stress. Cleavage cracks initiated in association with this crack-ring extend into the centre zone and fracture can be propagated from the centre zone completely through the surrounding area to initiate overall fracture. The effect of surface flaws on the fracture of laser-irradiated discs was observed to be small for randomly oriented scratches having widths of 60  $\mu\text{m}$ , depths of approximately 6  $\mu\text{m}$ , and lengths of 1 cm. While there was some interaction of these scratches with the central cleavage-fracture zone, the major causes of crack development and propagation were observed to be involved with intrinsic decohesion associated with the cleavage planes, and this feature was observed to be enhanced by cleavage-oriented scratches or scratches deviating by  $\sim 5^\circ$  or less from a cleavage direction. Intrinsic fracture was enhanced in the test material by the presence of numerous precipitates possessing long-range strain fields which, in some cases, were observed to generate linear arrays of overlapping strain fields whose function, it is believed, could be considered tantamount to an internal flaw of finite dimension-extending as much as 100  $\mu\text{m}$  in some cases.

Advancing crack-tips were observed directly in the transmission electron microscope and shown to have associated with them arrays of partial and total dislocations, in agreement with classical theories of brittle fracture, which postulate the presence of dislocations to advance the crack tip [17].

Coupling of laser-induced cracks with flaws has not been observed to be experimentally significant, except where the flaws are oriented in or near a cleavage direction. This may be due in part to the shallow and irregular nature of the scratches. Nonetheless, the results demonstrate that the effect of random scratches on a material such as silicon, or typically a brittle material susceptible to cleavage fracture, may be of little consequence when compared with internal, structural defects such as precipitates, or even with the intrinsic nature of cleavage.

### Acknowledgements

This research was supported by the Air Force Special Weapons Center (PMRB), Kirtland Air Force Base, Albuquerque, New Mexico under contract F29601-73-C-0126. The authors are

grateful to Dr C. Stein for his encouragement and the provision of facilities, and to C. J. Miglionico for his skilful operation of the scanning electron microscope. We are especially grateful for the technical assistance of Margaret L. Sattler. The comments and suggestions of the reviewer were also helpful in arriving at this final version of the manuscript.

### References

1. B. M. ASHKINADZE, V. I. VLADIMIROV, V. A. LIKHACHER, S. M. RYVKIN, V. M. SALMANOV and I. D. YAROSHETSKII, *Sov. Phys. J.E.T.P.* **23** (1966) 788.
2. G. I. BARENBLATT, O. E. MARIN, N. F. PILIPETSKII and V. A. UPADYSHEV, *ibid* **27** (1968) 716.
3. H. S. DODDS, J. E. FIELDS and A. H. MAITLAND, *Phil. Mag.* **28** (1973) 33.
4. P. B. WITHERS and T. R. WILSHAW, *J. Phys. D: Appl. Phys.* **6** (1973) 322.
5. P. V. AVIZONIS and T. FARRINGTON, *Appl. Phys. Letters* **7** (1965) 205.
6. M. B. AGRANAT, F. N. CHERNYHUSKY, N. P. NOVIKOV, S. S. SALVENYA, P. A. YAMPOLSKY, and YU. I. YUDIN, *Nature* **226** (1970) 349.
7. L. S. GOURNAY, *J. Acous. Soc. Amer.* **40** (1966) 1322.
8. B. STEVERDING, *J. Phys. D: Appl. Phys.* **3** (1970) 358.
9. N. C. ANDERHOLM, *Appl. Phys. Letters* **16** (1970) 113.
10. M. SPARKS, *J. Appl. Phys.* **44** (1973) 4137.
11. W. A. SZILVA, L. E. MURR and M. SATTLER, *J. Mater. Sci.* **9** (1974) 859.
12. L. E. MURR and R. T. PAYNE, *J. Appl. Phys.* **44** (1973) 1722.
13. S. TIMOSHENKO, "Strength of Materials", Part 2 (Van Nostrand, New York, 1947) p. 263.
14. R. J. SHAFFER, L. E. MURR, M. E. HANSON, A. G. PETSCHER and W. A. SZILVA, Final Report, Contract F29601-73-C-0126, AF Special Weapons Center (PMRB), Kirtland AF Base, Albuquerque, N.M. (1974).
15. L. E. MURR, "Electron Optical Applications in Materials Science" (McGraw-Hill, New York, 1970).
16. H. BETHGE, "Electron Microscope 1974: Proceedings of the VIII International Congress, Vol. 1, Physical", edited by J. V. Sanders and D. J. Goodchild (The Australian Academy of Science, Canberra, Australia, 1974) p. 724.
17. H. LIEBOWITZ, (ED.), "Fracture", Vols. VI and VII (Academic Press, New York, 1968, 1969).

Received 15 January and accepted 21 February 1975.